NUMERICAL SIMULATION OF ICING ON NREL 5-MW REFERENCE OFFSHORE WIND TURBINE BLADES UNDER DIFFERENT ICING CONDITIONS

Abstract: Offshore wind energy resources are operational in cold regions, while offshore wind turbines will face the threat of icing. Therefore, it is necessary to study icing of offshore wind turbines under different icing conditions. In this study, icing sensitivity of offshore wind turbine blades are performed using a combination of FLUENT and FENSAP-ICE software, and the effects of liquid water content (LWC), medium volume diameter (MVD), wind speed and air temperature on blade icing shape are analyzed by two types of ice, namely rime ice and glaze ice. The results show that the increase of LWC and MVD will increase the amount of ice that forms on the blade surface for either glaze ice or rime ice, and an increase of MVD will expand the adhesion surface between ice and blade. Before reaching the rated wind speed of 11.4 $m \cdot s^{-1}$, the wind speed does not directly affect the icing shape. However, after reaching the rated wind speed, the angle of attack of the incoming flow decreases obviously, and the amount of ice increases markedly. When the ambient air temperature meets the icing conditions of glaze ice (i.e., 0 to −5 ℃), the lower the temperature, the more that glaze ice freezes, whereas air temperature has no impact on the icing of rime ice. Compared with onshore wind turbines, offshore wind turbines have unique meteorological conditions, and the wind speed has no impact on the amount of ice that forms on the blade surface under most wind speed conditions.

Keywords: Environmental parameters; Cold regions; offshore wind turbine; Rime; Glaze; numerical simulation.

1. Introduction

Energy supply, environmental pollution, and global warming represent major global problems. Much attention has focused on the transition from nonrenewable energy resources (e.g., nuclear power, coal, and petroleum) to renewable energy resources (e.g., ocean, wind, and solar energy)(Fronk et al., 2010; Franchi et al., 2007). In 2020, global renewable energy capacity increased by more than 260 GW, which is nearly 50% higher than the increase in 2019. Furthermore, around 80% of all new electricity generating capacity is renewable (Whiteman et al., 2021). Renewable energy accounts for nearly 10% of electricity generation in most parts of the world, and it is expected to grow to meet 60% of global energy demand by 2050(Fronk et al., 2010). Among the various sources of renewable energy, wind energy has been most widely exploited. In 2020, global wind power capacity was approximately 733 GW, accounting for approximately 26% of renewable energy capacity, compared only 16% in 2011. Over the past 10 years, as the wind power industry has matured, offshore wind power has developed rapidly. At the end of 2020, global installed offshore wind capacity was more than 34 GW, i.e., 6 GW more than in 2019 and representing around an 11-fold increase from that in 2010 when the installed capacity was nearly 3 GW (Boshell et al., 2021). Additionally, the trend of development of offshore wind power is toward deep-sea, offshore, and high-power installations. For example, the Hywind Tampen floating offshore wind farm (in Norway) will be located 140 km from the coast in a sea area with depth of 260–300 m. Vestas recently announced the development of a 15-MW offshore wind turbine, which will be installed in 2022 and begin production in 2024 (Boshell et al., 2021).

Most northern regions of the world like arctic and clod regions have good wind resources. In 2017, the world's first offshore wind farm (Tahkoluoto offshore wind farm) designed for icing conditions was built in Finland. The wind farm is located in the Gulf of Bothnia at the northernmost end of the Baltic Sea. The wind farm is located close to the Arctic Circle in a harsh marine environment, which is of great relevance to the study of offshore wind turbine icing in cold areas. In this context, there will be more offshore wind farms in cold offshore environments, where the output efficiency and reliability of wind energy are mutually restricted. However, icing on wind turbines has been recognized as a hindrance to the development of the wind power in clod regions. In comparison with traditional onshore wind farms in cold climates, it will be more challenging to operate large wind turbines in cold offshore environments.

The blade is the most important component of a wind turbine, and icing on the blade (as shown in Fig. 1) could greatly degrade its aerodynamic performance, resulting in reduction of the power output (Botta et al., 1998). Additionally, icing could shorten the operational lifetime of a wind turbine by affecting its structural strength, which could also result in a potential safety hazard (Shi et al., 2016; Lu et al., 2009). Importantly, there is also the risk of ice throwing during operation of iced wind turbines, which could threaten the safety of maintenance personnel and other nearby structures (Morgan et al., 1998). Therefore, it is vital to investigate icing prediction methods and anti-icing/de-icing technology in relation to offshore wind turbine.

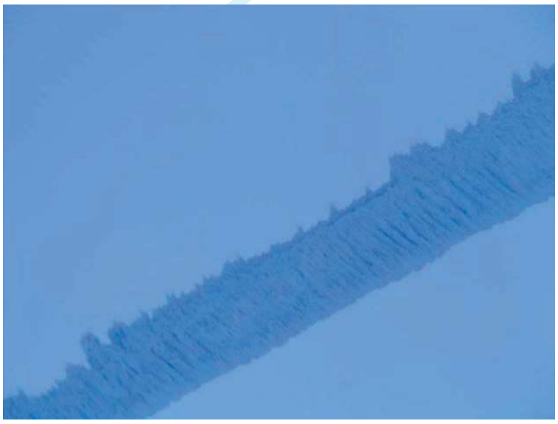

Fig. 1 Iced rotor blade (Battisti et al., 2006)

For accurate prediction of wind turbine icing, it is necessary to study the relevant environmental factors, e.g., air temperature, liquid water content (LWC), median volume diameter (MVD), and wind speed. Changes in these environmental parameters will affect the shape and type of icing of wind turbine blades, and degrade both the aerodynamic performance of the blades and the power output capacity of the turbines. Existing researches of icing forecasts have focused onshore wind turbine in cold regions, while comprehensive analysis of the more complex process of icing of an offshore wind turbine remains untouched. Therefore, this paper presents a numerical simulation study of icing of offshore wind turbines in cold regions with consideration of environmental factors.

In order to investigate the wind turbine blade icing, researchers have conducted relevant wind tunnel tests on wind turbine blades. For example, Li et al. (2014) conducted wind tunnel tests on wind turbine blades with the NACA7715 airfoil using a simple ice wind tunnel. They found that the area and rate of icing depend on the angle of attack and the wind speed, of which the relationship can be determined. Shin et al. (1992) performed a number of icing experiments to study the influence of different LWC, wind speed, and other parameters on icing of the NACA0012 airfoil. Bose (1992) researched horizontal-axis wind turbine with diameter of 1.05 m at icing environment, and identified the shape of glaze at different positions on the blade. It was found that glazing occurred primarily on the leading edge and tip of the blade. Guo et al. (2021) carried out an icing wind tunnel test of the straight-bladed vertical axis wind turbine with the NACA0018 airfoil under the different tip speed ratios and the rime ice condition. The research showed that the rotational speed of the blade has significant effects on the characteristics of icing.

Owing to its high costs, wind tunnel test has not been commonly applied in wind turbine icing research. Instead, numerical simulation methods have generally been adopted because they are more economical and effective. Numerical simulation of icing has also developed rapidly, and become the most widely used approach to study icing of wind turbine blades. The numerical simulation approach is inseparable from the icing model. There are currently two types of ice accumulation model in common use: empirical icing models and theoretical icing models. The former can produce icing results in a short time but with poor accuracy. The most typical example of an empirical icing model is the Makkonen model (Makkonen et al., 2001). This model is developed based on a quasi three-dimensional and flexible frame model, which is the basis of most other empirical icing models. Theoretical icing models can be categorized as either two-dimensional or three-dimensional blade icing models. Commercially available icing simulation software such as LEWICE, FENSAP-ICE, and TURBICE are all examples of such models. LEWICE is a two-dimensional model that is mainly used in the field of aviation, whereas TURBICE is a quasi three-dimensional model used mainly in the field of wind power generation. FENSAP-ICE is a three-dimensional model that is mainly used in the field of aviation and wind power generation. Two-dimensional and quasi three-dimensional icing calculation models only simulate a single airfoil without consideration of the influence of the three-dimensional flow. Quasi three-dimensional calculation models can incorporate complete blade icing. Although three-dimensional models can simulate the entire blade and consider the three-dimensional flow, they involve greater computational workload. Jasinski et al. (1998) investigated the effect on aerodynamic performance of rime ice accretion on the S809 wind turbine airfoil using LEWICE, and reported that icing can cause loss of aerodynamic performance of the airfoil. Barber et al. (2011) analyzed the influence of icing position of an airfoil on aerodynamic performance using LEWICE, and found that icing in the tip area of 95%–100% of the blade span has the most pronounced effect on the performance of a wind turbine. Muhammad et al. (2010) used TURBICE to study rime icing and the associated aerodynamic characteristics of four different wind turbine blade airfoils. Their results showed that the lift and drag coefficients of the blade airfoil increase with icing amount at the leading edge of the blade. Ibrahim et al. (2018) applied FENSAP-ICE to investigate the effects of LWC and temperature on blade icing and aerodynamic performance. The research finding showed that owing to blade icing, the lift coefficient was reduced by 10%–65%. Bai et al. (2021, 2022) analyzed the formation of ice on two major structural components of offshore platforms in Polar Regions using FENSAP-ICE, and it has been studied that icing characteristic under frost ice form on offshore turbine in cold regions.

The study of wind turbine icing usually needs to research atmospheric icing. Atmospheric icing occurs when supercooled cloud droplets come in contact with a surface which provides a crystallization site. So the research needs to study the meteorological conditions of Atmospheric icing. Most current research on the icing of wind turbines in cold areas still focuses on the effects of meteorological conditions over land. However, the meteorological conditions at sea are more complex, and relevant icing prediction methods need to be developed urgently. Moreover, when studying the working environment of wind turbines, most studies are based on wind tunnel parameters of previous tests rather than on actual parameters of cold areas. If environmental parameters are not combined with the actual working state of a wind turbine, and the simulated icing conditions are inconsistent with the actual conditions, it will be difficult to ensure the research conclusions. Additionally, when studying the icing under different conditions, existing studies have not clearly distinguished between the icing conditions of rime and glaze ice. With consideration of offshore wind turbine blades in cold areas, our study adopts a method combining FLUENT and FENSAP-ICE that incorporates arctic offshore climatic conditions and the actual working state of a wind turbine to analyze the influence of changes in environmental parameters on the icing shape of rime and glaze ice by changing environmental variables.

The remainder of this paper is structured as follows. Section 2 introduces the icing meteorological conditions and icing theory, including the icing mechanism and numerical simulation method. The numerical prediction method and its verification, including grid meshing and numerical verification, are presented in Section 3. Section 4 describes the effect of environmental parameters on icing, and analyzes the effects of LWC, MVD, temperature, and wind speed on icing. Sections 5 discusses the results of this study as compared with findings published in related literature, while Section 6 outlines the conclusions of this study and future improvement.

2. Icing meteorological conditions and theory

2.1 Icing meteorological conditions

In this study, the marine meteorological conditions in the arctic region were selected to analyze the impact of such conditions on wind turbine icing. Xie et al. (2001) studied the mechanism and physical characteristics of sea fog formation during China's first Arctic expedition. Chen et al. (2019) analyzed the characteristics of sea fog during a circumpolar expedition using navigation observational data obtained during China's eighth Arctic expedition. Both Arctic scientific surveys highlighted the importance of temperature and wind speed in the formation of sea fog in the Arctic. Makkonen (1984) summarized the LWC and MVD conditions of Arctic sea fog and considered that a height of 16 m above sea level is the upper limit of sea spray. At its lowest point, the blade tip of the offshore wind turbine considered in this study is nearly 30 m above sea level (as shown in Fig. 2); therefore, the impact of sea spray on blade icing was neglected. Consequently, the main consideration of this study was the impact of sea fog on the icing of an offshore wind turbine. Table 1 presents the typical meteorological conditions of icing in the Arctic.

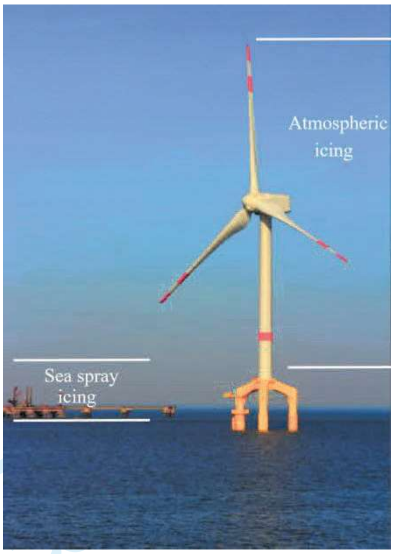

Fig. 2 Ice accumulation regions of an offshore wind turbine (Boshell et al.,2021)

Table 1 Meteorological conditions of icing in the Arctic

Temperature /°C	Wind speed /m·s^{-1}	LWC /(g·m^{-3})	MVD /μm	Air density / (kg·m^{-3})	Air viscosity / (m^2·s^{-1})
-15~0	≤13	0.04~0.20	4~20	1.293	1.7162×10^{-5}

2.2 Icing mechanism and simulation

2.2.1 Icing mechanism

Icing is a common natural phenomenon. From the perspective of thermodynamics, water becomes supercooled when its temperature drops below 0 °C. Supercooled water is not stable, but exists in a metastable state. The lifting of this state requires the formation of ice nuclei larger than a critical size. When an ice core larger than the critical size appears in supercooled water, the icing process begins. This ice core then grows within the supercooled water and finally becomes ice in the macro sense. During the operation of a wind turbine, icing will occur when the temperature around the blade surface is <0 °C and the blade collides with supercooled water droplets. In the icing process, owing to complex heat and mass transfer phenomena, supercooled water droplets impacting the blade surface will produce convective heat transfer, evaporation and sublimation, and release of latent heat, which together with external conditions will determine whether liquid water reflux is produced on the frozen surface (Kostinski et al., 2008; Debenedetti et al., 2003; Fortin et al., 2009).

On the basis of its characteristics, ice is usually divided into rime ice, glaze ice, and mixed ice; rime ice and glaze ice are generally the most typical types.

Rime ice mainly occurs when the ambient air temperature is low (usually lower than −5 °C) and the LWC and MVD values are small. Under these conditions, supercooled water droplets that hit the surface of a turbine blade will freeze immediately. The heat released during the icing process is insufficient to raise the temperature of the blade surface above freezing point; thus, the supercooled water droplets all frozen and there is no runback water. Therefore, regular and opaque icing occurs in the narrow area of the leading edge of the blade. Rime ice is generally divided into hard rime and soft rime. Hard rime generally has granular, white or translucent characteristics, the density is 600~900 kg/m^3. While soft rime generally has white or opaque characteristics, the density is 100–600 kg/m^3.

Glaze ice is generally formed when the ambient air temperature is relatively high (lower than 0 °C and higher than −5 °C) and the LWC and MVD values are relatively large. Under these conditions, supercooled water droplets do not freeze completely on contact with a structural surface; instead, they diffuse at the edge of the structural surface and refreeze in the adjacent areas to form ice with irregular edges and corners. In comparison with rime ice, glaze ice is stronger, more irregular in shape, and more difficult to remove (Battisti, 2015).

Mixed ice is a combination of rime and glaze ice formations. It occurs in layers from rime to glaze ice (Ozcan et al., 2021).

This study focused mainly on rime ice and glaze ice. The relationship between ice type, air temperature, and wind speed is shown in Fig. 3. At present, the offshore wind turbine industry uses this figure for the classification of ice types. Both DNV GL (DNVGL-RP-0175, 2017) and ISO (ISO 12494, 2017) have listed this figure as the icing standard for offshore wind turbines.

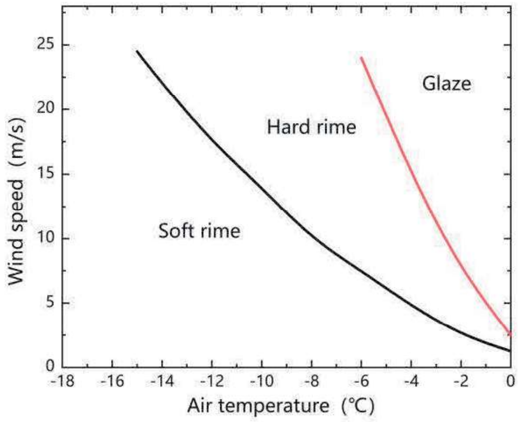

Fig. 3 Relationship between ice type, air temperature, and wind speed (ISO 12494, 2017)

2.2.2 Icing numerical simulation

The numerical simulation method is widely used to calculate icing. Such an approach generally comprises three steps: calculation of the flow field, calculation of water droplet trajectory, and calculation of ice growth.

1) Blade flow field calculation. The flow field distribution around a turbine blade is calculated to obtain parameters such as the air velocity around the blade.

The governing equation is the low-speed viscous flow Navier–Stokes equation, which is expressed as follows in its general form:

$$\frac{\partial \rho\phi}{\partial t} + \nabla(\rho \boldsymbol{v}\phi - \Gamma_{\phi} grad\phi) = q_{\phi} . \tag{1}$$

The continuity equation is

$$\frac{\partial \rho}{\partial t} + \nabla(\rho \boldsymbol{v}) = 0 , \tag{2}$$

where ρ is air density, t is time, ϕ is the transportation variable, $\boldsymbol{v}$ is air velocity, Γ_{ϕ} is a diffusion coefficient, and q_{ϕ} is the source item.

When the wind turbine is operating, the blade is in a rotating state, and the air is in a complex flow state. Therefore, blade element momentum theory is used to solve the influence of blade rotation and multiple blades on the flow field.

Blade element momentum theory (Ingram, 2005) is the main method used to analyze the aerodynamic performance of wind turbine blades. The movement of air around a blade is a complex flow with vortexes. Blade element momentum theory divides the wind turbine blade into multiple micro segments in the span-wise direction. These micro segments are blade elements that reflect the changes of axial and tangential velocity of the air flow by introducing axial and tangential induction factors. Through this method, analysis based on the principle of momentum conservation and aerodynamic theory is possible.

In the process of numerical simulation, there are two important parameters: the relative wind speed (V_{rel}) and the angle of attack (α_0). These parameters depend on the incoming wind speed (V_∞), axial and tangential induction factors (a and b), section radius (r), local speed ratio (λ_r), and blade twist angle at this section (φ), as shown in Fig. 4. The relative wind speed and angle of attack of each section can be calculated using the following formulas (Muhammad et al., 2012; Matthew et al., 2012):

$$V_{rel} = \sqrt{\left(V_\infty\left(1-a\right)\right)^2 + \left(\frac{\lambda_r r}{V_\infty}\right)^2}, \tag{3}$$

$$\alpha_0 = \arctan\left(\frac{1-a}{\lambda_r\left(1+b\right)}\right) - \varphi, \tag{4}$$

where

$$\lambda = \frac{\pi n R}{30V_\infty}, \lambda_r = \frac{\lambda r}{R}, \tag{5}$$

$$a = \frac{1}{\left(1+\frac{8\pi r\cos^2\beta_0}{BcC_L\sin\beta_0}\right)}, \tag{6}$$

$$b = \frac{BcC_L}{2\pi r\cos\beta_0}(1-a), \tag{7}$$

where R is the rotor radius, C_L is the lift coefficient, B is the number of blades, c is the chord length of the blade airfoil, λ is the tip velocity ratio, and $\beta = 90 - \alpha_0 - \varphi$ is the angle of the relative wind.

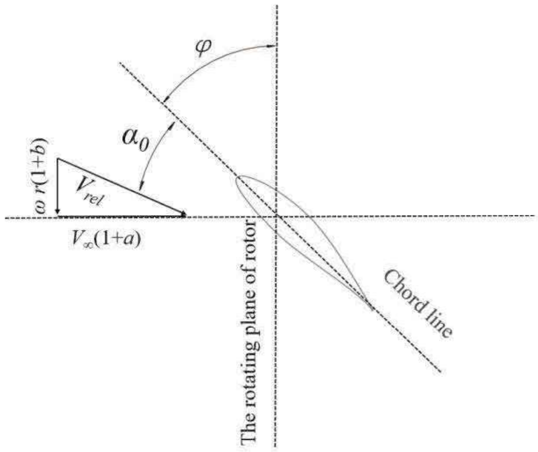

Fig. 4 Diagram of blade element momentum theory (here, pitch angle = 0)

2) Droplet trajectory calculation. The DROP3D module in FENSAP-ICE software was used for the calculation of water drop trajectory. On the basis of the calculation results of the blade flow field, the motion equation of the supercooled water drops is solved, and each water drop is tracked to determine whether it collides with the blade. The gas–liquid two-phase control equation is established using the Euler method, and then the control equation is solved using the finite volume method to obtain the trajectory of the water droplets and the impact characteristics of the blade surface.

Water droplet trajectory motion equation:

$$\frac{\partial \alpha}{\partial t} + \nabla(\alpha \boldsymbol{u}_d) = 0, \tag{8}$$

$$\frac{\partial \boldsymbol{u}_d}{\partial t} + \boldsymbol{u}_d \nabla \boldsymbol{u}_d = \frac{C_D Re_d}{24K}(\boldsymbol{u}_a - \boldsymbol{u}_d) + (1 - \frac{\rho_a}{\rho_d})\frac{1}{Fr^2}\boldsymbol{g}, \tag{9}$$

$$Re_d = \frac{\rho_a d V_{rel} \left\| \boldsymbol{u}_a - \boldsymbol{u}_d \right\|}{\mu_a}, \tag{10}$$

$$K = \frac{\rho_d d^2 V_{rel}}{18 \mu_a L_\infty}, \tag{11}$$

$$Fr = \frac{\left\| V_{rel} \right\|}{\sqrt{L_\infty g_\infty}}, \tag{12}$$

$$C_D = \begin{cases} 24 / Re_d \left(1 + 0.15 Re_d 0.687\right) & Re_d \le 1300 \\ 0.4 & Re_d > 1300 \end{cases}, \tag{13}$$

where K is the inertia factor, Fr is the Froude number, C_D is the resistance coefficient, α is the volume fraction of water droplets, $\boldsymbol{u}_a$ and $\boldsymbol{u}_d$ are air velocity and water droplet velocity, respectively, μ_a is the kinematic viscosity of air, L_∞ is the characteristic length, and $\boldsymbol{g}$ is the reference gravity.

3) Ice growth calculation. The ice growth calculation uses the ICE3D module in FENSAP-ICE. This module uses the Bourgault icing model, solves the icing thermodynamic model of the blade surface using mass and energy conservation equations, and obtains the distribution of blade surface temperature and icing amount.

When the icing type is glaze ice.

Mass conservation equation:

$$\rho_f\left[\frac{\partial h_f}{\partial t}+\nabla\cdot\left(\bar{V}_f h_f\right)\right]=V_{rel}LWC\beta-m_{evap}-m_{ice}, \tag{14}$$

Energy conservation equation:

$$\begin{aligned}\rho_f\left[\frac{\partial h_f c_f T_f}{\partial t}+\nabla\cdot\left(\bar{V}_f h_f c_f T_f\right)\right]&=\left[c_f(T_\infty-T_f)+\frac{\|V_d\|^2}{2}\right]V_{rel}LWC\beta-L_{evap}m_{evap}\\&+(L_{fusion}-cT)m_{ice}+\sigma\varepsilon(T_\infty^4-T_{f4}),\\&-c_h(T_f-T_{ice,rec})+Q_{anti-icing}\end{aligned} \tag{15}$$

where f is the water film; m_{evap} is the evaporative mass flux; m_{ice} is the ice accretion mass flux; ρ_f, c_f, c_s, ε, σ, L_{evap}, and L_{fusion} represent physical properties of the fluid; $Q_{anti-icing}$ is the anti-icing heat flux. The specific expression of each item and the detailed solution method of the equations can be found in Bourgault et al. (2000) and ANSYS FENSAP-ICE User Manual (2020).

When the icing type is rime ice, the droplets will freeze directly when they hit the blade surface, meaning that it is not necessary to consider heat transfer and phase transformation but only mass conservation. Thus, the mass conservation equation can be written as follows:

$$V_{rel} LWC \beta = m_{ice} \text{,} \tag{16}$$

$$\boldsymbol{V}_{ice} = \frac{m_{ice}}{\rho_{ice}} \boldsymbol{n} = \frac{V_{rel} LWC_{\infty} \beta}{\rho_{ice}} \boldsymbol{n} \text{,} \tag{17}$$

$$\Delta h_{ice} = \frac{m_{ice}}{\rho_{ice}} \Delta t \text{,} \tag{18}$$

where ρ_{ice} is ice density, Δt is the time step, $\boldsymbol{V}_{ice}$ is the ice growth rate, Δh_{ice} is the ice surface displacement, and $\boldsymbol{n}$ is the surface normal vector.

2.2.3 Calculation process

This study combined FLUENT and FENSAP-ICE to perform numerical simulation of the icing of wind turbine blades. The section grid of a clean airfoil was generated using ICEM software. This grid was imported into FLUENT to analyze the flow field around the blade. The results of the flow field analysis were imported into FENSAP-ICE. In FENSAP-ICE, the DROP3D module calculated the droplet trajectories, and the ICE3D module calculated the icing growth and derived the airfoil form after icing. Because rime ice and glaze ice form mainly at the leading edge of an airfoil, the grid of the leading edge of the airfoil needs to be densified. The frozen airfoil section grid, generated in ICEM, was imported into FLUENT, and the above process was repeated until the specified criteria for ending the process were realized. A schematic of the calculation process is presented in Fig. 5.

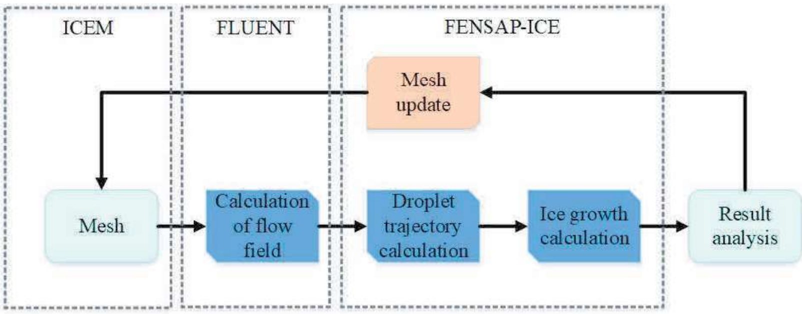

Fig. 5 Flowchart of the calculation process

3. Numerical prediction method and verification

3.1 Computational domain and meshing

In this study, a single blade (length: 61.5 m) of the NREL 5-MW offshore wind turbine (Jonkma et al., 2009) was selected for use in the calculation. Icing in the tip area of 95%–100% of the blade span has greatest impact on aerodynamic performance (Barber et al., 2011). In this study, the blade micro segment located 61.63 m from the rotor root of the wind turbine blade was used as the research object. The airfoil was the NACA64-A17, which has chord length of 1.419 m (see Fig. 6).

Simulation of both clean airfoils and airfoils with ice adopt the C-type structured grid in ANSYS ICEM (see Fig. 7). Each boundary is more than 20 times the chord length from the airfoil. The left boundary of the calculation domain is the velocity inlet, the right boundary is the pressure outlet, and the solid wall surface of the airfoil adopts a nonslip wall surface. To accurately determine the flow characteristics of the boundary layer, the y+ values near the airfoil surface are <10, and the height of the first layer on the wall is set at 1.0×10^{-5}, using the K- ω SST turbulence model.

Table 2 Distributed blade aerodynamic properties (data from Jonkma et al., 2009)

Node	Blade Radial Location (m)	Aerodynamic Twist (°)	Chord Length (m)	Airfoil Table
1	2.8667	13.308	3.542	Cylinder1
2	5.6000	13.308	3.854	Cylinder1
3	8.3333	13.308	4.167	Cylinder2
4	11.7500	13.308	4.557	DU40-A17
5	15.8500	11.480	4.652	DU35-A17
6	19.9500	10.162	4.458	DU35-A17
7	24.0500	9.011	4.249	DU30-A17
8	28.1500	7.795	4.007	DU25-A17
9	32.2500	6.544	3.748	DU25-A17
10	36.3500	5.361	3.502	DU21-A17
11	40.4500	4.188	3.256	DU21-A17
12	44.5500	3.125	3.010	NACA64-A17
13	48.6500	2.319	2.764	NACA64-A17
14	52.7500	1.526	2.518	NACA64-A17
15	56.1667	0.863	2.313	NACA64-A17
16	58.9000	0.370	2.086	NACA64-A17
17	61.6333	0.106	1.419	NACA64-A17

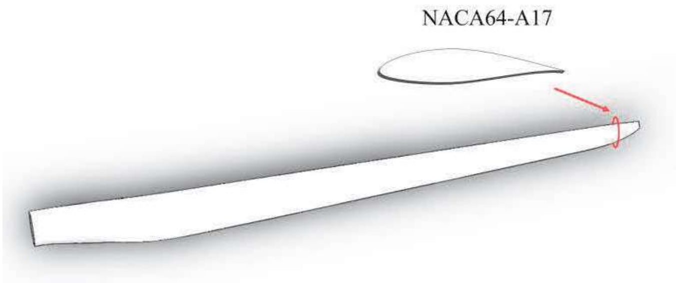

Fig. 6 Blade model

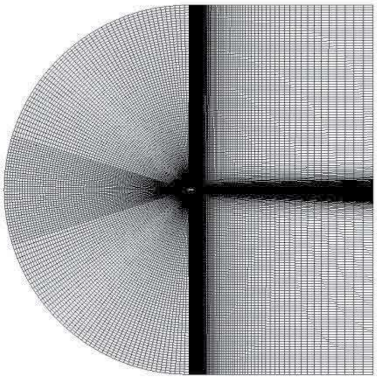

(a) Grids in computational zone

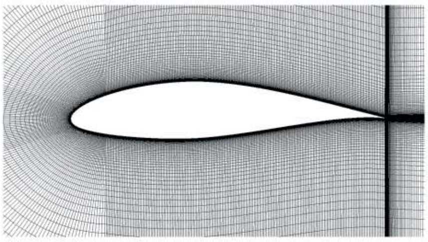

(b) Partial grid of a clean airfoil

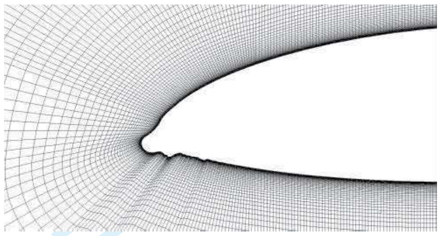

(c) Partial grid of an iced airfoil

Fig. 7 Grids in the computational zone and partial grids of the airfoil

3.2 Numerical method validation

To verify the accuracy of the numerical simulation results, the derived simulation results were compared with experimental results. Of these, the numerical simulation of NACA0012 airfoil icing is a classic example that incorporated rich ice wind tunnel test data. Shin J et al. (1992) conducted many ice wind tunnel tests on NACA0012 airfoil icing at the Lewis Research Center of NACA, from which they obtained a large volume of test data. In this study, two groups of test results were selected for comparative analysis to verify the accuracy of FENSAP-ICE with regard to icing under rime ice and glaze ice conditions.

The calculation conditions specified in the literature were as follows: airfoil chord length C = 0.5334 m, angle of attack AOA = 4 °, temperature T = −2.22 ℃ and T = −26.1 ℃, incoming flow velocity v = 67.05 m·s^{-1}, MVD = 20 μm, LWC = 1 g·m^{-3}, and icing time t = 360 s.

It can be seen from Fig. 8 that the ice shape predicted in this study is in good agreement with the experimental results. When the ice type is glaze ice, the edges and corners of the ice shape are largely the same, i.e., the growth direction is the same and the runback water range is similar. When the icing type is rime ice, the riming is concentrated mainly at the leading edge of the airfoil, the icing thickness is largely the same, and most of the ice shapes coincide. Thus, the above verifies the suitability of the calculation method adopted in this study.

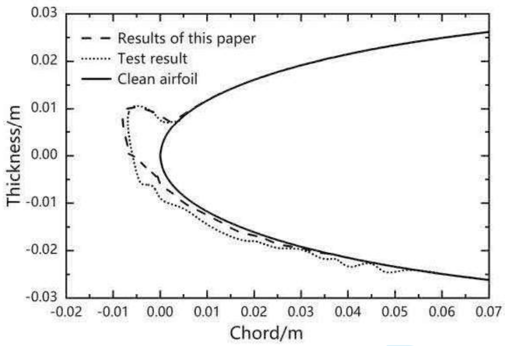

(a) Glaze ice

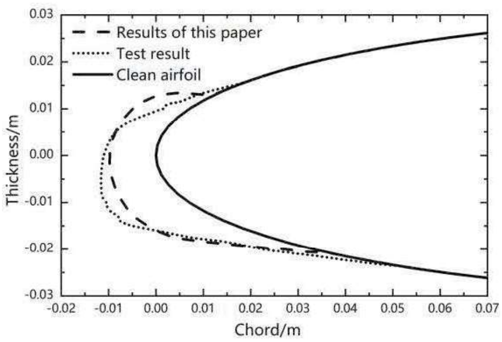

(b) Rime ice

Fig. 8 Comparison of ice shape simulated in this study and determined by experiment

4. Analysis of the effect of environmental parameters on icing

4.1 Calculation duration selection

arctic sea fog is the most important condition regarding icing of offshore structures. Sea fog can be categorized as advection fog, radiation fog, or vapor fog. Advection fog generally persists the longest, i.e., up to 24 h; radiation fog and vapor fog usually persist for only 1–3 h (Chen et al., 2019). In addition, two years of field data in northern Europe specified the icing duration frequency to be between 1 h and 4 h (Stoyanov et al., 2019). Therefore, to facilitate comparison of icing under different environmental conditions, the icing time selected in this study was 2 h.

4.2 Time step selection

In the calculation of the icing numerical simulation, the selection of time step influences the simulation results. Moreover, a change in the surface local collection coefficient β after airfoil icing also affects the results of the icing numerical simulation. In computational fluid dynamics analysis, the smaller the selected time step, the more accurate the calculation results. However, the process requires a high-performance computer and the calculation time increases as the time step is reduced; therefore, it is necessary to select an appropriate time step.

In this study, the conditions listed in Table 2 were adopted for the research, for which MVD was 20 μm, LWC was 0.2 $g \cdot m^{-3}$, icing time was 2 h, wind speed was 13 $m \cdot s^{-1}$, blade speed was 12.1 rpm, air temperature was –15 ℃, and all other icing conditions remained unchanged. The time steps adopted were 5, 15, and 30 min. Table 3 lists the numerical calculation results of the three different time steps. It can be determined that in comparison with the icing amount for a time step of 5 min, the percentage change in the amplitude of the icing amount for time steps of 15 and 30 min was 1.38% and 5.67%, respectively. The simulation results produced using the various time steps were similar, but with increased icing time, the change in the increase of icing amount for the time steps of 15 and 30 min was greater in comparison with that of the 5 min time step. Therefore, considering the calculation efficiency and accuracy achieved with the various time steps, a time step of 15 min was selected in this study.

Table 3 Numerical calculation results of icing for three time steps

Time step（min）	Icing amount（kg）
5	0.06657
15	0.06749
30	0.07034

4.3 Effects of different icing conditions on different icing types

4.3.1 Effect of different icing conditions on glaze icing

Five groups of data with LWC of 0.04, 0.08, 0.12, 0.16, and 0.20 g·m^{-3} were selected. The icing time was 2 h, MVD was 20 μm, wind speed was 13 m·s^{-1}, blade speed was 12.1 rpm, air temperature was −3 °C, and all other icing conditions remained unchanged. The icing shapes produced by different LWCs under the icing conditions of glaze ice are shown in Fig. 9.

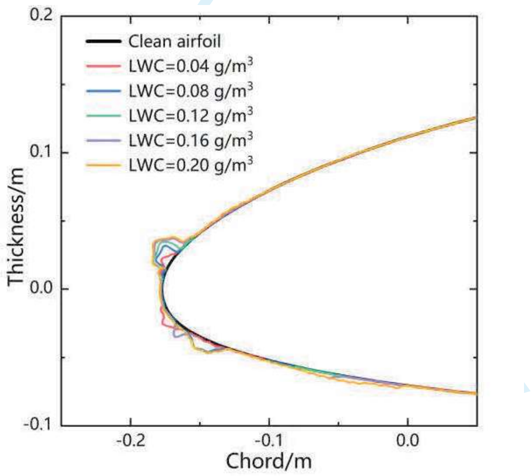

Fig. 9 Shapes of glaze icing on blade surface produced under different liquid water content (LWC)

Five groups of data with MVD of 4, 8, 12, 16, and 20 μm were selected. The icing time was 2 h, LWC was 0.2 g·m^{-3}, wind speed was 13 m·s^{-1}, blade speed was 12.1 rpm, air temperature was −3 °C, and other icing conditions remained unchanged. The icing shapes produced by different MVDs under the icing conditions of glaze ice are shown in Fig. 10.

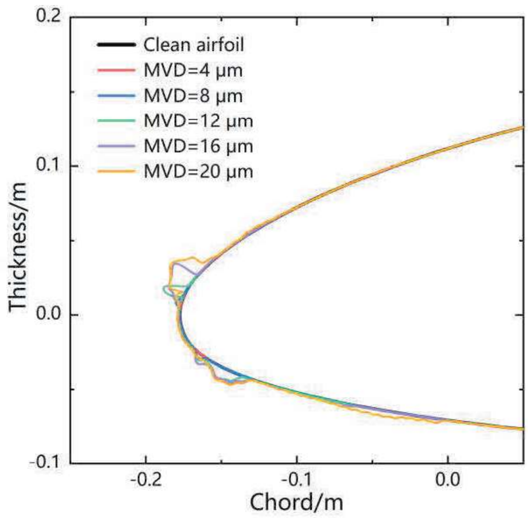

Fig. 10 Shapes of glaze icing on blade surface produced under different median volume diameter (MVD)

Four groups of data with wind speeds of 7, 9, 11, and 13 $m \cdot s^{-1}$ were selected. The icing time was 2 h, LWC was 0.2 $g \cdot m^{-3}$, MVD was 20 μm, air temperature was −3 °C, and other icing conditions remained unchanged. Table 4 lists the blade rotation speed and attack angle of the wind turbine blade under different wind speeds, the inlet velocity of the flow field is set according to the relative wind speed. Fig. 11 shows the icing shapes produced by different wind speeds under the icing conditions of glaze ice.

Table 4. Calculation parameters under different wind speeds

Wind speed/ $m \cdot s^{-1}$	3	5	7	9	11	13
Rotor speed /rpm	7	7.5	8.3	10.2	11.7	12.1
Attack angle /°	8.515	8.635	8.706	8.718	9.507	8.462
Relative wind speed / $m \cdot s^{-1}$	44.101	47.618	52.896	64.808	74.412	75.609

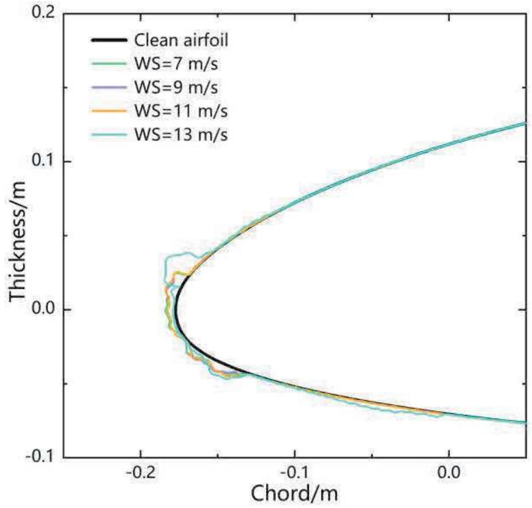

Fig. 11 Shapes of glaze icing on blade surface under different wind speeds

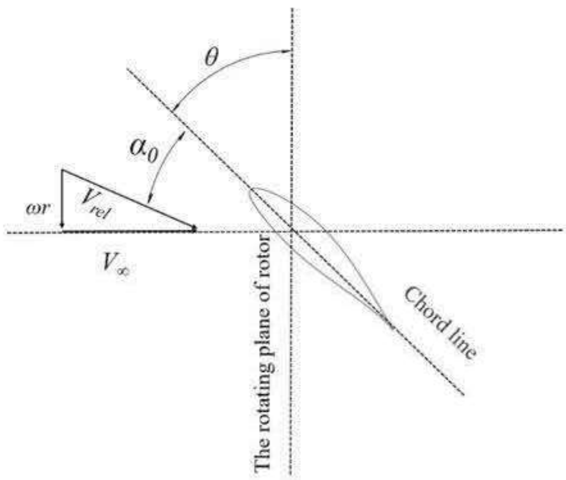

Fig. 12 Relationship between relative wind speed and pitch angle (Here, twist angle is 0°)

Table 5 Sensitivity of aerodynamic power to blade pitch (data from Jonkma et al., 2009)

Wind Speed ($m \cdot s^{-1}$)	Rotor speed (rpm)	Pitch Angle (°)	Wind Speed ($m \cdot s^{-1}$)	Rotor speed (rpm)	Pitch Angle (°)
11.4-Rated	12.1	0.00	19.0	12.1	16.23
12.0	12.1	3.83	20.0	12.1	17.47
13.0	12.1	6.60	21.0	12.1	18.70
14.0	12.1	8.70	22.0	12.1	19.94
15.0	12.1	10.45	23.0	12.1	21.18
16.0	12.1	12.06	24.0	12.1	22.35
17.0	12.1	13.54	25.0	12.1	23.47
18.0	12.1	14.92			

Four groups of data with air temperatures of −1, −2, −3, and −4 °C were selected. The icing time was 2 h, LWC was 0.2 g·m^{-3}, MVD was 20 μm, wind speed was 13 m·s^{-1}, blade speed was 12.1 rpm, and other icing conditions remained unchanged. The icing shapes produced by different temperatures under the icing conditions of glaze ice are shown in Fig. 13.

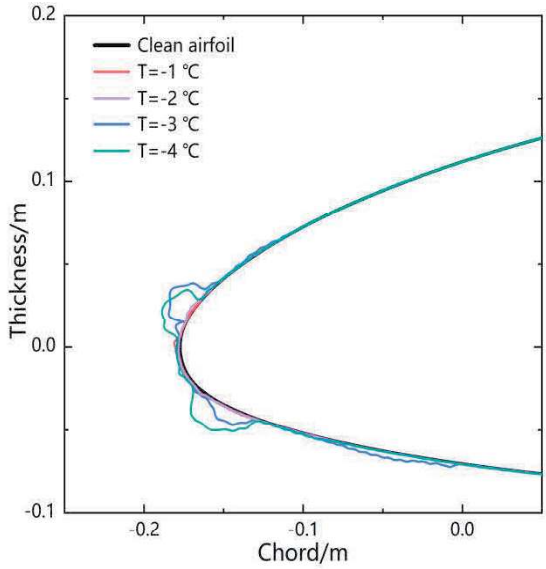

Fig. 13 Shapes of glaze icing on blade surface under different air temperatures

It can be seen from Fig. 9 to Fig. 13. Under the condition of glaze ice, the amount of icing on the blade surface gradually increases with the increase of LWC and MVD. the runback water phenomenon is more obvious with the increase of LWC. the icing and airfoil attachment surface tend to expand gradually with the increase of MVD. the icing shape does not change notably with the increase of wind speed. air temperature change has substantial impact on icing shape. The lower the temperature, the more ice that forms on the blade surface, and the less obvious the runback water phenomenon.

4.3.2 Effect of different icing conditions on rime icing

Five groups of data with LWC of 0.04, 0.08, 0.12, 0.16, and 0.20 g·m^{-3} were selected. The icing time was 2 h, MVD was 20 μm, wind speed was 13 m·s^{-1}, blade speed was 12.1 rpm, air temperature was −15°C, and all other icing conditions remained unchanged. The icing shapes produced by different LWCs under the icing conditions of rime ice are shown in Fig. 14.

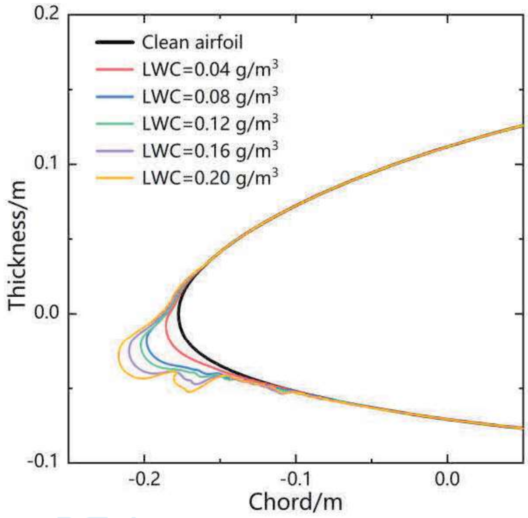

Fig. 14 Shapes of rime icing on blade surface produced under different liquid water content (LWC)

Five groups of data with MVD of 4, 8, 12, 16, and 20 μm were selected. The icing time was 2 h, LWC was 0.2 g·m^{-3}, wind speed was 13 m·s^{-1}, blade speed was 12.1 rpm, air temperature was −15 ℃, and other icing conditions remained unchanged. The icing shapes produced by different MVDs under the icing conditions of rime ice are shown in Fig. 15.

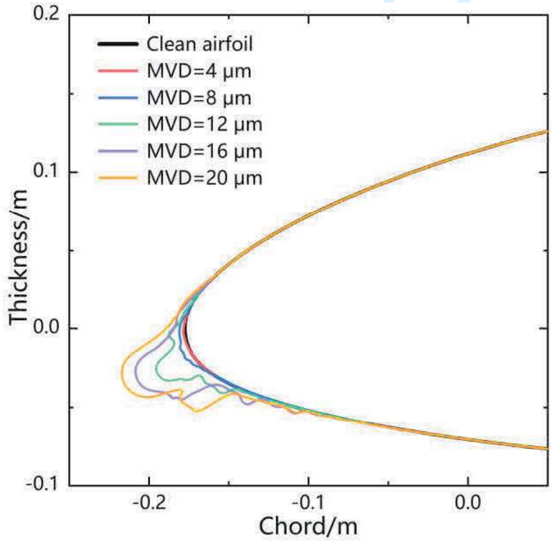

Fig. 15 Shapes of rime icing on blade surface produced under different median volume diameter (MVD)

Six groups of data with wind speeds of 3, 5, 7, 9, 11, and 13 $m\cdot s^{-1}$ were selected. The icing time was 2 h, LWC was 0.2 $g\cdot m^{-3}$, MVD was 20 μm, air temperature was −15 ℃, and other icing conditions remained unchanged. Table 4 lists the blade rotation speed and attack angle of the wind turbine blade under different wind speeds, the inlet velocity of the flow field is set according to the relative wind speed. Fig. 16 shows the icing shapes produced by different wind speeds under the icing conditions of rime ice.

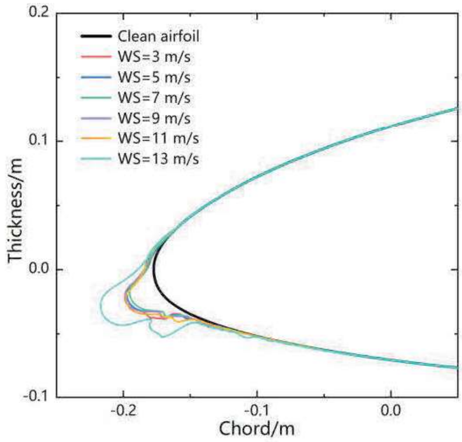

Fig. 16 Shapes of rime icing on blade surface under different wind speeds

Four groups of data with air temperatures of −6, −9, −12, and −15 ℃ were selected. The icing time was 2 h, LWC was 0.2 $g\cdot m^{-3}$, MVD was 20 μm, wind speed was 13 $m\cdot s^{-1}$, blade speed was 12.1 rpm, and other icing conditions remained unchanged. The icing shapes produced by different temperatures under the icing conditions of rime ice are shown in Fig. 17.

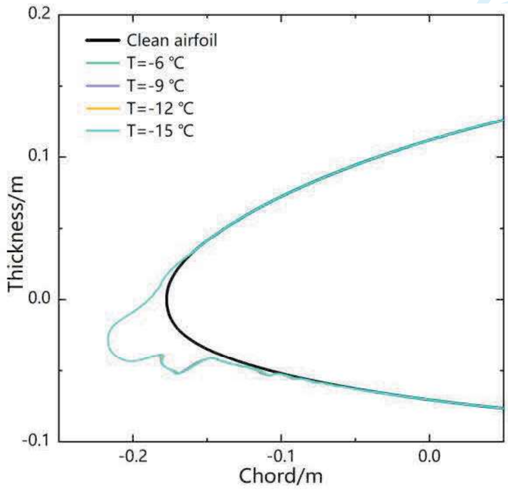

Fig. 17 Shapes of rime icing on blade surface under different air temperatures

It can be seen from Fig. 14 to Fig. 17. Under the condition of rime ice, the amount of icing on the blade surface gradually increases with the increase of LWC and MVD. the ice edges and corners become more prominent with the increase of LWC and MVD. the icing and airfoil attachment surface tend to expand gradually with the increase of MVD. the icing shape does not change notably with the increase of wind speed. the icing shape does not change with the decrease of temperature.

4.3.3 Effect analysis on icing conditions

LWC represents the mass of liquid water contained in unit volume of air. Under the same other conditions, increase of LWC means there would be more water droplets in unit volume of air. Thus, more water droplets would be available to hit the blade surface, more liquid water would be collected in the micro elements of the blade surface, and in the subsequent mass and heat transfer process, it would freeze to form more ice.

Under the same other conditions, the inertia of a single water droplet increases with the increase of the average water droplet diameter. When a larger droplet approaches the blade surface, this inertia means the magnitude of its deviation from the streamline is increased, and it is easier for it to hit the blade surface, so that more liquid water is collected in the micro elements of the blade surface, and the attachment surface between the ice and the airfoil is expanded.

The icing shape does not change notably with the increase of wind speed for either glaze ice or rime ice, except at the wind speed of 13 $m\cdot s^{-1}$. The main reason for this phenomenon is that before reaching the rated rotor speed of the wind turbine, the speed of rotor changes linearly with wind speed, and the change of the incoming attack angle is not obvious. When the wind speed reaches the rated wind speed of 11.4 $m\cdot s^{-1}$, the speed of the rotor remains unchanged at 12.1 rpm (as shown in Table 5). At this moment, the incoming attack angle changes greatly in comparison with the previous attack angle and therefore the ice shape also changes. The parameter that most affects the icing shape is not a single wind speed. With a change of wind speed (before reaching the rated wind speed), the rotor speed increases, but the pitch angle is 0° (as shown in Fig. 12 and Table 5), and the relative speed and angle of attack also increase; therefore, the icing shape does not change. After reaching the rated wind speed of 11.4 m·s^{-1}, the rotor speed remains unchanged at 12.1 rpm, its pitch angle increases, the relative speed increases slightly, but the angle of attack decreases (as shown in Table 4); therefore, the icing shape changes markedly. In summary, wind speed does not directly affect the icing shape on a wind turbine blade, but its quasi synthetic relative speed and angle of attack can affect the icing shape.

Temperature has different effects on glaze and rime. This is because under the condition of glaze ice, higher temperatures mean it is more difficult for water droplets in the air to freeze immediately on contact with the blade surface, and it is more difficult for water droplets to adhere to the blade surface. Therefore, when the air temperature is relatively low, more ice forms on the blade surface. Under the condition of rime ice, the change of air temperature has no obvious effect on icing shape. This is because under the condition of rime ice, water droplets freeze immediately when they hit the blade surface. When the LWC in the air, the MVD, and other environmental parameters remain unchanged, the icing shape remains consistent under the same icing time.

4.3.4 Analysis on boundary between glaze and rime ice in ice type selection

In Figure 3, when the icing condition is at the boundary between glaze and rime ice, the type of icing is actually difficult to determine. Therefore, there is insufficient analysis in sections 4.3.1 and 4.4.2. In this section, the ice type selection at the ice type boundary will be different from sections 4.3.2 and 4.4.3.

In Figure 11, when the icing condition is near the boundary line, the ice type is glaze ice, while in this section the ice type is rime ice. Five groups of data with wind speeds of 3, 5, 7, 9, and 11 m·s^{-1} were selected. and other icing conditions remained unchanged. Fig. 18 shows the icing shapes produced by different wind speeds under the icing conditions of rime ice (when the temperature is –3 ℃).

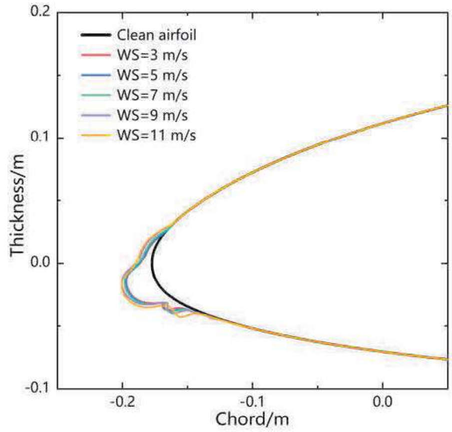

Fig. 18 Shapes of rime icing on blade surface under different wind speeds (T=−3 ℃)

In Figure 12, when the icing condition is near the boundary line, the ice type is glaze ice, while in this section the ice type is rime ice. Six groups of data with wind speeds of −3, −4, −6, −9, −12and −15 ℃ were selected. and other icing conditions remained unchanged. Fig. 19 shows the icing shapes produced by different air temperatures under the icing conditions of rime ice.

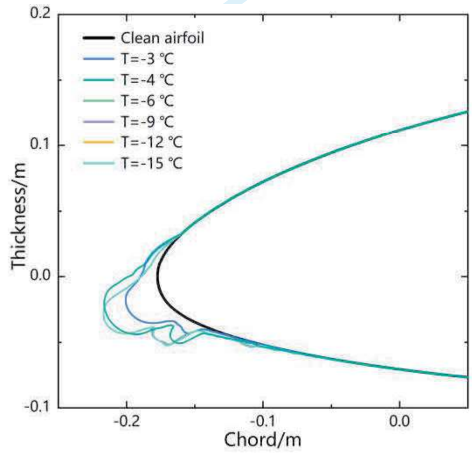

Fig. 19 Shapes of rime icing on blade surface under different air temperatures

It can be seen from Fig. 18, When the wind speed is lower than 9 $m \cdot s^{-1}$, the icing shape does not change notably with the increase of wind speed. When the wind speed reaches 11 $m \cdot s^{-1}$, the icing shape changes slightly. The main reason for this change is that the ice type at this wind speed may be the icing condition of glaze ice. Therefore, Under the condition of rime ice, the change of wind speed does not change the icing shapes.

In Fig. 19, When the temperature is higher than −5 °C, the amount of ice is significantly reduced. At this temperature, water droplets will not freeze immediately when they hit the blade surface. Ice at this temperature cannot meet the requirements of rime ice, ice melts at this temperature. Technically, the ice formed at this temperature is not rime ice. However, when the temperature is lower than −5 °C, the amount of ice does not change. Therefore, Under the condition of rime ice, the change of temperature does not change the icing shapes.

Therefore, the conclusions in section 4.3.3 on air temperature and wind speed under glaze ice or rime ice conditions are still valid.

5. Discussion

In this section, the numerical simulation results of this study, presented in Section 4, are discussed through comparison with the results of Etemaddar et al. (2014). The NREL 5-MW wind turbine adopted for analysis in Etemaddar et al. (2014) is comparable with the turbine considered in this study. It was used to simulate atmospheric icing of a wind turbine in a cold area and to conduct sensitivity research. The selected sensitivity parameters were angle of attack, relative wind speed, characteristic length, airfoil, temperature, LWC, MVD, and relative humidity. The environmental parameters of wind speed, temperature, LWC, MVD, and relative humidity represent the biggest difference in sensitivity studies of offshore and onshore wind turbines. According to Etemaddar et al. (2014), relative humidity has no effect on icing; therefore, this discussion considers only the four environmental parameters of wind speed, temperature, LWC, and MVD.

The environmental parameters selected in the literature represent average values with typical variational ranges measured over the past few decades. The icing time was 2 h, and each parameter was evenly distributed. The specific ranges of the environmental parameters are listed in Table 6.

Table 6 Meteorological conditions considered in Etemaddar et al. (2014)

T/°C	Relative wind speed /($m\cdot s^{-1}$)	LWC/($g\cdot m^{-3}$)	MVD/μm
-10~0	20~100	0.05~0.25	8~24

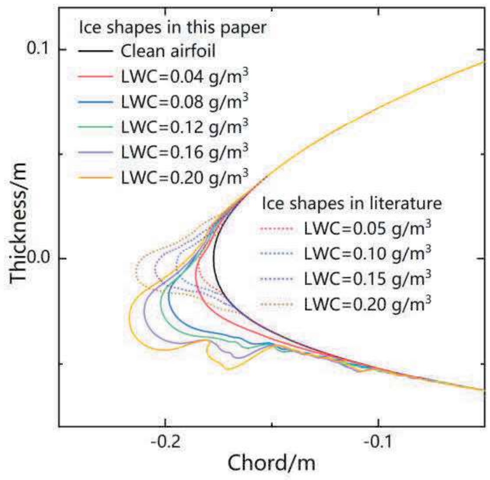

Fig. 20 Effect of liquid water contents (LWC) on ice profile

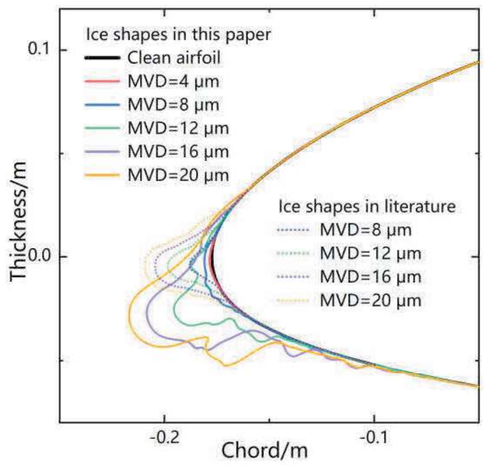

Fig. 21 Effect of median volume diameter (MVD) on ice profile

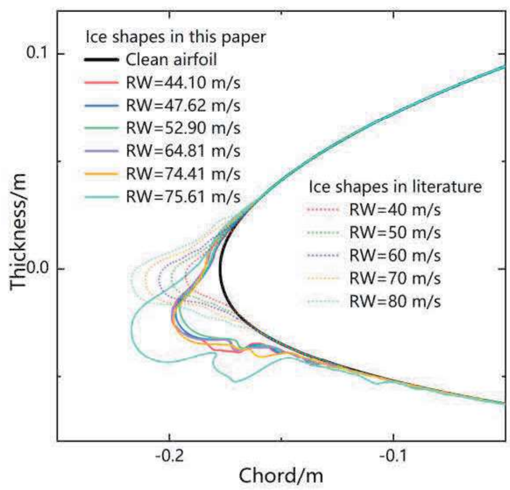

Fig. 22 Effect of relative wind speed on ice profile

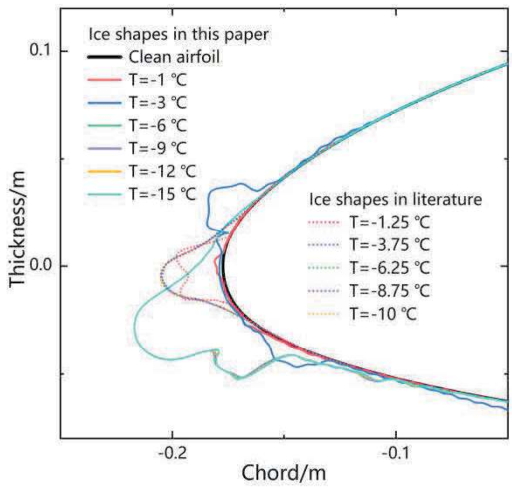

Fig. 23 Effect of temperature on ice profile

It can be seen from Fig. 20 that the icing is typical of rime ice. Although the other environmental parameters are different, it can be determined that with the increase of LWC in the air, the amount of icing on the blade surface gradually increases, and the icing and airfoil attachment surface do not change.

The icing in Fig. 21 is typical of rime ice. Similar to the conclusions reached in relation to Fig. 15, with the increase of MVD, the amount of icing on the blade surface gradually increases, and the icing and airfoil attachment surface also expand.

The influence of relative wind speed on icing is shown in Fig. 22. However, the relative wind speed is determined by the wind speed and the linear velocity of the position of the airfoil, and the change of these two parameters affect the angle of attack of the incoming flow. Therefore, during actual operation of a wind turbine, it is impossible to study the influence on icing by controlling the single variable of relative wind speed. However, it can be determined from Fig. 22 that the incoming flow velocity increases and that the amount of ice on the blade surface also gradually increases.

The effect of air temperature on icing is shown in Fig. 23. It can be seen that although there are differences in the environmental parameters and the distinguishing temperature between rime ice and glaze ice, the conclusion is similar to that reached in relation to Fig. 13 and Fig. 17, i.e., the change of air temperature has no obvious effect on the shape of rime ice.

When the ambient temperature is lower, the amount of glaze ice on the blade surface also increases gradually, and the runback water phenomenon is no more obvious.

By comparing the conclusions reached in this paper with those in the literature, it can be seen that the most obvious difference lies in the consideration of icing type. When studying the influence of sensitivity on icing, two types of icing (i.e., rime ice and glaze ice) are considered in this paper, whereas only typical rime ice was considered in the literature. This study demonstrated that certain differences will become apparent between rime ice and glaze ice with the change of individual environmental parameters. Moreover, this study considered the environmental parameters of specific locations, whereas the parameters adopted in Etemaddar et al. (2014) were average values and typical variational ranges measured over the past few decades, which might not necessarily coexist in reality. For example, under certain wind speed conditions, LWC might not reach the value studied. Finally, when studying the influence of sensitivity on icing, only the airfoil was studied in Etemaddar et al. (2014), i.e., the actual working environment of the wind turbine was neglected. For example, in actual operation of a wind turbine, to achieve maximum energy capture efficiency, the angle of attack will be changed by pitch during operation to maximize the lift–drag ratio of the blade airfoil. The variational range of the lift–drag coefficient with the angle of attack of the NACA64-A17 airfoil considered in Jonkma et al. (2009) is shown in Fig. 24. It can be seen that when the angle of attack is approximately 10°, the lift–drag ratio of this airfoil reaches its maximum, and the angle of attack listed in Table 4 is approximately in this range. However, the angle of attack selected in the literature was always 0°, which is inconsistent with the actual operating conditions of a wind turbine. The above differences have greater impact in relation to subsequent research on the prediction of wind turbine icing, the aerodynamic performance of icing blades, the power output of wind turbines, the icing environment when the wind turbine is parking, and the anti-icing and de-icing of wind turbines.

The current study has certain shortcomings. First, when studying the effect of air temperature on icing, the coexistence of rime ice and glaze ice might occur under certain temperature conditions, i.e., mixed ice. The influence of this atypical icing type on icing is not considered in this paper. Second, when studying the impact of wind speed on icing, it was found that wind speed does not directly change the icing shape, but that the synthetic relative speed and angle of attack can affect the icing shape. Limited by information regarding the wind speed conditions of offshore icing environments, this study also failed to deliver a conclusion on the trend of change of icing after the rated wind speed is reached, which is a subject that should be studied in detail considering the expected subsequent change of icing environment conditions.

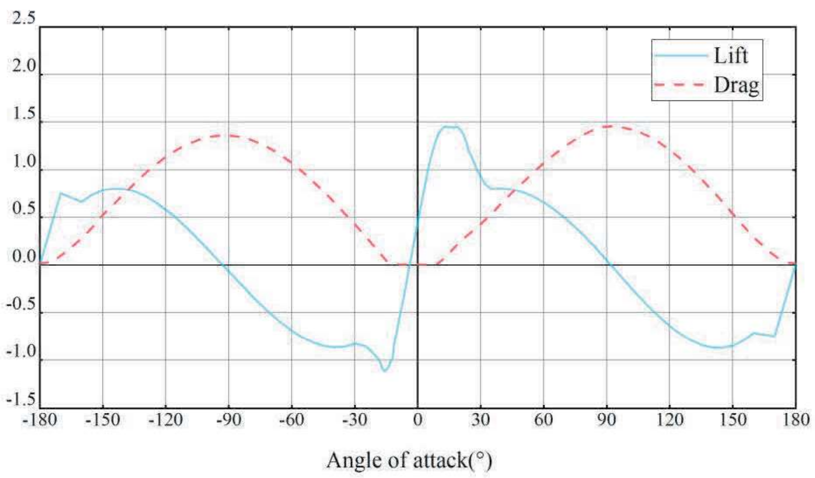

Fig. 24 Coefficients of the NACA64-A17 airfoil (data from Jonkma et al., 2009)

6. Conclusions

With the development of the wind power industry, more offshore wind turbines will be installed in the future. Offshore wind turbines will face the threat of winter icing, which will directly affect their operation. Therefore, it is necessary to study predictions of icing of offshore wind turbines. The meteorological conditions of traditional wind turbine icing prediction research are generally based on the land environment, and do not include the actual working state of a wind turbine; thus, the derived conclusions are not necessarily applicable to offshore wind turbines. Therefore, it is highly important that research be conducted on icing under different icing conditions with consideration of the actual working state and working environment of offshore wind turbines.

In this study, numerical simulation of icing on offshore wind turbine blades was performed using a combination of FLUENT and FENSAP-ICE software, and the icing under different icing conditions was studied. The derived conclusions are as follows.

1) The LWC and MVD, have an effect on the icing shape of glaze ice and rime ice. When LWC is in the range of 0.05–0.25 $g \cdot m^{-3}$ and MVD is in the range of 8–24 μm, increase of LWC and MVD will increase the amount of ice that forms on the blade surface. A change of LWC does not change the adhesion surface between the ice and the blade, whereas an increase of MVD will expand the adhesion surface between ice and blade.

2) Before reaching the rated wind speed of 11.4 $m \cdot s^{-1}$, the wind speed does not directly affect the icing shape of glaze ice and rime ice. However, after reaching the rated wind speed, the angle of attack of the incoming flow decreases obviously, and the amount of glaze ice and rime ice increases markedly. Due to the existence of sea fog, the wind speed when the blade of offshore wind turbine icing may not reach the wind speed when it icing on land. This is the most obvious difference between offshore and onshore wind turbine icing.

3) A change in ambient air temperature has considerable impact on the icing of glaze ice, but has no impact on the icing of rime ice. When the ambient air temperature meets the icing conditions of glaze ice (i.e., 0 to −5 °C), the lower the temperature, the more that glaze ice will freeze.

4) This study investigated the icing of blade on offshore wind turbines under different icing conditions, mainly under typical icing conditions of glaze ice and rime ice. However, the actual icing environment is highly complex, and temperature change over a short period could lead to the formation of mixed ice. Therefore, research on icing type must be improved.

5) When studying the impact of wind speed on blade icing, it was found that the incoming angle of attack and the relative velocity have direct impact on icing shape, but under the limiting meteorological conditions of sea fog, wind speed must be <13 $m \cdot s^{-1}$. In this context, the variation of wind turbine angle of attack and relative velocity is limited, which is not conducive to study of the impact of the change of angle of attack and relative

velocity on icing. Therefore, the wind turbine environment could be changed in the future to study the joint effects of angle of attack and relative speed on icing.

REFERENCE

ANSYS FENSAP-ICE User Manual, 2020. ANSYS 2020 R2. ANSYS, Inc. Canonsburg, PA.

Bai X., Shen J., Xue Y. Z., et al., 2021. Numerical Forecasting of Icing on Structural Components of Offshore latforms in Polar Regions [J]. China Ocean Engineering, Vol.35, No.4, P. 588-597.

Barber S., Wang Y., Jafari S., et al., 2011. The Impact of Ice Formation on Wind Turbine Performance and Aerodynamics [J]. Journal of Solar Energy Engineering, 133(1):011007.

Battisti L., Fedrizzi R., Brighenti A., et al., 2006. Sea ice and icing risk for offshore wind turbines [J]. Owemes, April 20-22.

Battisti L., 2015. Wind Turbines in Cold Climates: Icing Impacts and Mitigation Systems [M]. Green Energy and Technology, Springer International Publishing, Switzerland.

Bose N, 1992. Icing on a small horizontal-axis wind turbine—Part 1： Glaze ice profiles[J]. Journal of wind engineering and industrial aerodynamics, 45(1): 75-85.

Boshell F., Ocenic E., Abunofal M. et al., 2021. Offshore renewables: An action agenda for deployment[R]. International Renewable Energy Agency.

Botta G., Cavaliere M., Holttinen H., 1998. Ice accretion at Acqua Spruzza and its effects on wind turbine operation and lose of energy production[C]. Proceeding of the International Conference.

Bourgault Y., Beaugendre H., Habashi W., 2000. Development of a Shallow Water Icing Model in FENSAP-ICE[J]. Journal of Aircraft , 37(4): 640 –646.

Chen Z. K., Wei L. X., Li Z. Q., et al., 2019. Sea fog characteristics over the Arctic pack ice in summer 2017[J]. Marine forecasts, 36(2):77-87. (in china)

Debenedetti P. G., Stanley H. E., 2003. Supercooled and Glassy Water [J]. Journal of Physics: Condensed Matter, 45: 40-46.

DNVGL-RP-0175, 2017, Icing of wind turbines[S]. Oslo: DNV GL copyright office.

Etemaddar M., Hansen M. O. L., Moan T., 2014. Wind turbine aerodynamic response under atmospheric icing conditions [J]. Wind energy, 17: 241-265.

Fortin G, Perron J., 2009. Wind Turbine Icing and De-Icing [R]. AIAA 2009-274.

Franchi J. R., Mokhatab S., 2007. Energy: Technology and Directions for the Future [J]. Journal of Energy Resources Technology, 129(1):79-79.

Fronk B. M., Neal R., Garimella S., 2010. Evolution of the Transition to a World Driven by Renewable Energy [J]. Journal of Energy Resources Technology, 132(2):021009.

Guo W. F., Shen H., Li Y., Feng F., et al., 2021. Wind tunnel tests of the rime icing characteristics of a straight-bladed vertical axis wind turbine[J]. Renewable Energy, Volume 179, 116-132.

Ibrahim G. M., Pope K., Muzychka Y. S., 2018. Effects of blade design on ice accretion for horizontal axis wind turbines [J]. Journal of wind engineering and industrial aerodynamics, 173: 39-52.

Ingram G., 2005. Wind turbine blade analysis using the blade element momentum method[D]. Durham University: Durham, NC, USA.

ISO 12494 :2017. Atmospheric icing of structures[S]. Switzerland: ISO copyright office.

Jasinski W. J., Noe S. C., Selig M.S., et al., 1998. Wind turbine performance under icing conditions[J]. Journal of energy engineering, 120(1): 60-65.

Jonkma J. M., Butterfield S., Musial W., et al., 2009. Definition of a 5-MW Reference Wind Turbine for

Offshore System Development[J]. Technical Report NREL/TP-500-38060, National Renewable Energy Laboratory, Golden, CO, USA.

Kostinski A., Cantrell W., 2008. Entropic aspects of supercooled droplet freezing [J]. Journal of the Atmospheric Sciences, 65:2961-2871.

Li Y., Tagawa K., Feng F., et al., 2014. A wind tunnel experimental study of icing on wind turbine blade airfoil [J]. Energy Conversion and Management, 85:591-595.

Lu B., Li Y., Wu Z., 2009. A review of recent advances in wind turbine condition monitoring and fault diagnosis [J]. IEEE Power Electronics and Machines in Wind Applications, 1-7.

Ozcan Y., Ismail H. T., 2021. Aerodynamic shape optimization of wind turbine blades for minimizing power production losses due to icing [J]. Cold Regions Science and Technology, Volume 185.

Makkonen L., 1984. Atmospheric icing on sea structures [J]. CRREL report documentation number, 84-2.

Makkonen L., Laakso T., Marjaniemi M., et al., 2001. Modelling and prevention of ice accretion on wind turbines[J]. Wind Engineering, 25: 3-21.

Matthew C., Homola, Muhammad S. V., et al., 2012. Performance losses due to ice accretion for a 5 MW wind turbine[J]. Wind energy, 15: 379-389.

Morgan C., Bossanyi E., Seifert H., 1998. Assessment of safety risks arising from wind turbine icing [J]. Wind Energy Prod Cold Clim, 113-121.

Muhammad S. V., Matthew C., Homola, et al., 2010. Effect of Rime Ice Accretion on Aerodynamic Characteristics of Wind Turbine Blade Profiles [J]. Wind Engineering, 34(2): 207-218.

Muhammad S. V. ,Matthew C., Homola, et al., 2012. Atmospheric icing on large wind turbine blades[J]. International journal of energy and environment, 3(1):1-8.

Shi W., Tan Z., Moan T., 2016. Numerical study of ice-induced loads and responses of a monopole-type offshore wind turbine in parked and operating conditions [J]. Cold regions science and technology, 121-139.

Shin J., Bond T. H., 1992. Results of an Icing Test on a NACA0012 Airfoil in the NASA Lew is Icing Research Tunnel [M]. National Aeronautics and Space Administration.

Shin J, Bond T. H., 1992. Experimental and Computational Ice Shapes and Resulting Drag Increase for a NACA0012 Airfoil[R]. NASA TM-105743.

Stoyanov D.B., Nixon J.D., Sarlak H., 2021. Analysis of derating and anti-icing strategies for wind turbines in cold climates[J]. Applied Energy, Volume 288,116610.

Whiteman A., Akande D., Elhassan N., et al., 2021. Renewable Energy Capacity Statistics[R]. International Renewable Energy Agency.

Xie S. M., Xue Z. H., Qu S. H., et al., 2001. Summer arctic sea fog [J]. Acta oceanologica sinica, 23(6):40-50. (in china)

Yang X., Bai, X., Cao H., 2022. Influence analysis of rime icing on aerodynamic performance and output power of offshore floating wind turbine [J]. Ocean Engineering, 258, 111725.